

Pose Refinement with Joint Optimization of Visual Points and Lines

Shuang Gao[†], Jixiang Wan[†], Yishan Ping[†], Xudong Zhang^{*}, Shuzhou Dong, Jijunnan Li, Yandong Guo

Abstract—High-precision camera re-localization technology in a pre-established 3D environment map is the basis for many tasks, such as Augmented Reality, Robotics and Autonomous Driving. The point-based visual re-localization approaches are well-developed in recent decades, but are insufficient in some feature-less cases. In this paper, we propose a point-line joint optimization method for pose refinement with the help of the innovatively designed line extracting CNN named VLSE, and the line matching and pose optimization approach. We adopt a novel line representation and customize a hybrid convolutional block based on the Stacked Hourglass network, to detect accurate and stable line features on images. Then we apply a coarse-to-fine strategy to obtain precise 2D-3D line correspondences based on the geometric constraint. A following point-line joint cost function is constructed to optimize the camera pose with the initial coarse pose. Sufficient experiments are conducted on open datasets, i.e, line extractor on Wireframe and YorkUrban, localization performance on Aachen Day-Night v1.1 and InLoc, to confirm the effectiveness of our point-line joint pose optimization method.

I. INTRODUCTION

Re-localization technology based on visual features is widely used in the field of Computer Vision, such as Augmented Reality, Indoor Navigation, Mobile Robots and Autonomous Driving [1] [2]. The essence of visual localization is to obtain the camera’s 6 degrees of freedom (DoF) including its position and orientation through the corresponding relationship between the captured image and the pre-established 3D environment map. Common visual features on images include points, lines, planes and some more advanced features, like semantic labels.

The visual localization based on point features thrives in recent years. A large number of visual point extractors [3] [4], matching methods [5] [6] and point-based 3D mapping approaches [7] [8] have been proposed. Although the visual points can lead to more accurate image positions, they are still sensitive to weak textures and illumination changes. In some cases, visual lines, containing more structured information, are more robust to these phenomena.

For visual line detection, traditional methods such as LSD [9], FLD [10] and EDlines [11] usually rely on low-level image gradients and edge features. Moreover, they also struggle to distinguish high-level local textures and structural elements. With the rapid advance of deep learning, the Convolutional Neural Networks (CNN) based line segment detection models have achieved superior performances over the traditional methods [12]–[20]. Supported by a large-scale dataset with manual wireframe annotations [12], we

succeed in training a deep model to capture structured and informative line segments (e.g., building contours, stairs), while ignoring line segments associated with texture (e.g., carpet patterns), which aims to lift the subsequent mapping and localization accuracy.

In this work, we also present a novel pose optimization method, that combines the advantages of both point and line in the localization task. The major idea of the point-line joint optimization method is to adjust poses by minimizing the reprojection error of point and line correspondences separately. In detail, a standard pose estimation method, Perspective-n-Point (PnP) [21] within a RANSAC loop [22], is employed to obtain an initial pose by utilizing 2D-3D point correspondences, and the inlier point correspondences are saved for subsequent optimization. The line segments on every image are extracted in both the mapping and localization stage. We innovatively design a CNN called VLSE to extract the visual lines. And the coarse-to-fine line matching correspondences will be acquired based on the initial pose and 3D line map. Finally, a point-line joint optimization cost function is employed to improve the accuracy of the final pose estimation.

In this paper, we conclude our contributions on the camera pose optimization by using point and line features mainly into the following parts:

1. We propose a more accurate visual line detection CNN named VLSE, where we utilize an innovative line segment representation and a customized hybrid convolutional block based on the Stacked Hourglass network [23].
2. We design a coarse-to-fine line matching method based on initial pose, which takes advantage of epipolar geometry hints and reprojection filtering to select high-quality line match pairs.
3. We adopt a point-line joint optimization cost function containing a more accurate line reprojection error measurement method to obtain the final high-precision pose.

II. RELATED WORKS

In this section, we introduce some recent progress in visual line extraction methods, line matching approaches and line-based visual localization researches. All of them are highly related to our work on point-line optimization on the pose refinement task.

Deep Line Segment Detection. [12] provides a large public dataset with wireframe annotations and a heuristic wireframe fusion algorithm, which makes the learning-based line segment detection task possible. Moreover, [13] and [14] train end-to-end neural networks to filter the wrong predicted

[†] Authors contributed equally to this work.

^{*} indicates corresponding author. Contact: zhangxudong@oppo.com

All authors are with OPPO Research Institute, Shanghai, China.

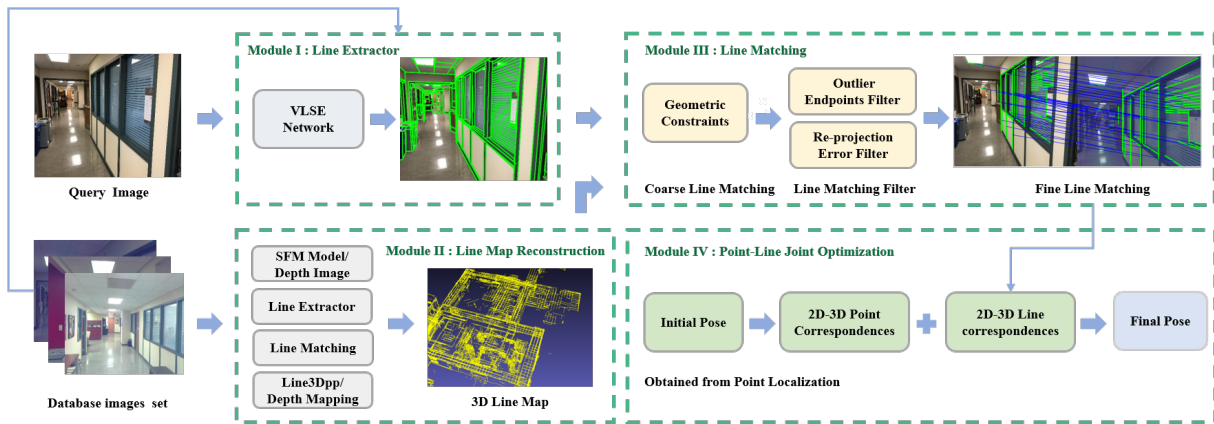


Fig. 1. **Point-Line Joint Pose Optimization Pipeline.** The input data contains database images set for mapping, query image with initial pose and 2D-3D point correspondences from the initial pure point-based localization. Module I is visual line extraction for subsequent line matching and mapping. The output of Module II is a 3D line map reconstructed by SFM + Line3Dpp or depth images + depth mapping. Module III is a coarse-to-fine line matching and its input contains 2D lines from Module I, a 3D line map from Module II and the initial pose of the query image. Module IV is point-line joint optimization.

endpoints in the junction heatmap. [16] integrates AFM-based reparameterization scheme [15] for line segments, and significantly improves both accuracy and efficiency. Recently, [17]–[20] directly encodes a line segment into several parameters predicted directly from the networks, without heuristics-driven line proposal generation, and further simplify the architecture.

Line Matching. The line matching methods can be roughly divided into two categories. As to traditional line matching methods, [24] applies the epipolar geometry and compute the overlapping score between the reference and candidate line segments. [25] uses the innovatively designed tensor to describe the lines and match them between images. [26] proposes the line band descriptor based on line appearance similarity, and the K Nearest Neighbors (KNN) match method can be used for matching. For the learning-based line matching method, [27] uses a graph convolution network to match line segments. [28] proposes a self-supervised occlusion-aware line description and detection method. Many methods face great difficulties in precision, especially when there is great viewpoint change or large-scale change between the matching image pairs.

Line Localization. For visual localization problems based on the line features, there are several works combining point features and line features in recent years. [29] describes how straight lines can be added to a monocular Extended Kalman Filter Simultaneous Mapping and Localization (SLAM) system to provide good poses and mapping. [30]–[32] are PL-SLAM systems that defined distances from endpoints of 3D line to corresponding 2D line as line reprojection error. [33] proposes a tightly-coupled monocular visual-inertial-odometry system exploiting both point and line features. In [34], the camera poses and 2D-3D line correspondences are iteratively optimized by minimizing the projection error of correspondences and rejecting outliers, where the line reprojection error denotes the sum of distances from endpoints to the corresponding 2D line. In addition, a direct pose

estimation method using 2D-3D line correspondences named Perspective-n-Line (PnL) is proposed in [35].

III. PROPOSED APPROACH

Our pose refinement pipeline mainly consists of four parts: 2D line extractor, 3D line map reconstruction, line matching and filtering, point-line joint optimization, which is illustrated in Fig.1.

Line extractor. For line feature re-localization, an accurate and stable line extraction method is needed. Extracted line features on the database for mapping and on query images for 2D-3D line matching are detected by performing our innovative CNN named VLSE described in III-A.

Line map reconstruction. According to the different characteristics of the datasets, the 3D line map is reconstructed using different strategies. For datasets that can be sparsely reconstructed with points, we employ an existing method named Line3Dpp [36], based on SFM, while for datasets with depth images, we propose a light-weight reconstruction method which maps the 2D line to 3D space directly with outliers filter by PnP and RANSAC.

Line matching and filtering. The coarse 2D line matches between database image and query image are calculated by utilizing epipolar constraint based on the initial pose of query obtained from point localization. Then we map the 2D line on database image onto the 3D line map, and deny the line matches with large reprojection error.

Point-Line joint optimization. Given the initial pose and corresponding points matches from point localization, we implement a process to minimize reprojection error of point correspondences and line correspondences to make the final estimated pose more accurate.

The following contents are constructed as our three main contributions in the total pipeline: visual line segment extractor, line matching and filtering containing 3D line mapping, and pose refinement with point-line.

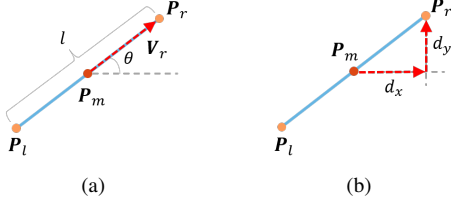


Fig. 2. **Line segment representation.** For a line segment, one of the endpoints P_r can be calculated with the absolute location of the midpoint P_m and its relative position relationship to the midpoint V_r , the other endpoint can also be determined by V_r in the opposite direction, due to the central symmetry of the two endpoints. (a) shows the traditional line representation with length l and angle θ . (b) shows the proposed line representation with horizontal and vertical distance d_x and d_y from right point to the midpoint.

A. VISUAL LINE SEGMENT EXTRACTOR

1) **Line Representation:** Inspired by [18], [19], we directly predict the locations of the two endpoints representing a single line segment as depicted in Fig.2, instead of proposing complicated line candidates using the line sampler in L-CNN [13]. P_l and P_r are the left and right endpoint of a certain line, while V_r is the vector representing the relationship between the P_r and the midpoint P_m . Usually, the length l and horizontal angle θ are used to produce the V_r [18], [19] as shown in Fig.2(a). However, the difficulties in predicting the accurate angle θ will result in large line errors especially for the prediction of a long line segment, because even a slight deviation of θ can have a great influence on the location of the endpoints. Such problems are relieved after we change to predict the pair of the horizontal distance $d_x = \frac{1}{2}(l \cos \theta)$, because the junctions' position offset distance errors are more discriminative than the angle error during the training stage. Furthermore, d_x and d_y are adopted to produce V_r instead of the pair of length l and θ , as shown in Fig.2(b). P_l and P_r are expressed by:

$$P_l = P_m - V_r, \quad P_r = P_m + V_r, \quad (1)$$

where P_l , P_m and P_r denote the coordinates of the left point, middle point and the right point of a 2D line, respectively.

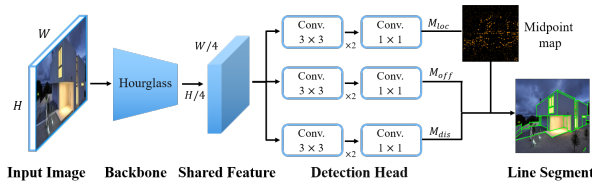


Fig. 3. **Architecture of VLSE network.** Stacked Hourglass network (HG) is chosen as our backbone to generate shared features. The following Convs are used to produce down-sampling and up-sampling features to form the midpoint map, and the line segment detection heads are used to construct the lines eventually.

2) **Line Segment Detection:** Fig.3 illustrates our proposed VLSE (Visual Line Segment Extractor) architecture. Which contains a feature extraction backbone and a line segment detection head. Stacked Hourglass network (HG) is chosen as our backbone to generate shared features, and it is

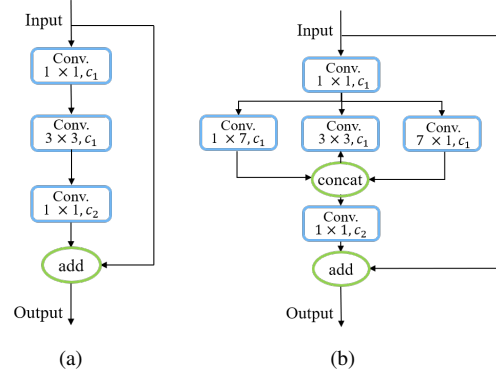


Fig. 4. **Line segment representation.** (a) is the basic convolutional block in HG and (b) is our customized hybrid convolutional block.

also adopted by L-CNN [13] and HAWP [16]. In which, the feature information at different scales is fused after a series of down-sampling and up-sampling. The basic convolution block of HG is shown in Fig.4(a), including two 1×1 convolution layers and one 3×3 convolution layer. Different from many other cases in Object Detection tasks, the length of the support region along the line's direction vector is much larger than the width of the region along the line's normal vector. Therefore, we additionally design two slender and long convolution kernels (e.g., 7×1 and 1×7). Drawing on the idea of Inception [37], the computational results from them are concatenated with the original 3×3 convolution (as illustrated in Fig.4(b)), as a way to fuse the visual features extracted from different receptive fields. After the backbone, the shared feature map, denoted by \mathcal{F} , is produced in the size of $H/4 \times W/4 \times 128$ with respect to the input image in the size of $H \times W \times 3$.

By feeding shared feature map \mathcal{F} into the line segment detection head, we can further compute line segment proposals by predicting the midpoints and the locations of the corresponding endpoints. Let M_{loc} in Fig.3 be the 2-D map representing the likelihood map, which means whether each sub-pixel contains a midpoint or not. Then the midpoint confidence map can be calculated followed by a Softmax layer. In order to restore the pixel-level midpoint prediction in the original image, an additional 2-D map M_{off} is also introduced to form the local offsets of the midpoints, just like the junction predictions as intended in [13], [16]. We adopt a sigmoid activation to normalize M_{off} to the boundary with $[0, 1) \times [0, 1)$. The third 2-D map M_{dis} can infer the endpoint displacements with respect to the midpoints in the horizontal and vertical directions.

B. LINE MATCHING AND FILTERING

A coarse-to-fine matching method using geometry constraint and reprojection filtration is proposed, which consists of coarse 2D-2D line matching, 3D line mapping and accurate 2D-3D line matching.

With the help of image retrieval [38], the image corresponding pairs are acquired, and line segments are extracted by CNN described in Section III-A. Inspired by [39], our

algorithm employs geometry constraints to obtain candidate line matches, which can be formulated by following:

$$\mathbf{l}'_l = \mathbf{F} * \mathbf{p}_q^l, \quad \mathbf{l}'_r = \mathbf{F} * \mathbf{p}_q^r, \quad (2)$$

$$\mathbf{l}_d = \mathbf{p}_d^l \times \mathbf{p}_d^r, \quad (3)$$

$$\mathbf{p}_l = \mathbf{l}_d \times \mathbf{l}'_l, \quad \mathbf{p}_r = \mathbf{l}_d \times \mathbf{l}'_r, \quad (4)$$

where \mathbf{F} represents the fundamental matrix produced by the initial coarse pose of query and ground truth pose of database. As is illustrated in Fig.5, \mathbf{l}_q and \mathbf{l}_d represent the line segments in the query image and the database image respectively. The \mathbf{p}_m^n ($m = q, d$ and $n = l, r$) represent homogeneous coordinates of the endpoints on the line segment. \mathbf{l}'_l and \mathbf{l}'_r represent the epipolar line corresponding to point \mathbf{p}_q^l and \mathbf{p}_q^r respectively. \mathbf{p}_l represents the intersect point of \mathbf{l}_d and \mathbf{l}'_l , \mathbf{p}_r represents the intersect point of \mathbf{l}_d and \mathbf{l}'_r . The overlapping ratio between the candidate matching lines will be computed [24], and the candidates reached a certain threshold are retained as the coarse line matches.

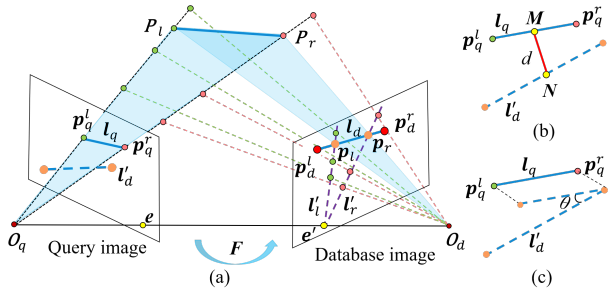


Fig. 5. **The process of line matching.** (a) is the process of coarse line matching using geometry and depth reprojection constraints. (b) and (c) are the method to acquire high-quality 2D-2D line matches. \mathbf{l}'_d is projected line through world line $P_l P_r$, point M and N represent the midpoint of line \mathbf{l}_q and \mathbf{l}_d respectively, d represents the distance between point M and point N , θ is defined as the angle between line \mathbf{l}_q and line \mathbf{l}'_d .

After the coarse 2D-2D line matches are obtained, we utilize the additional 3D line maps to established 2D-3D matches. For datasets with the SFM model, we employ an excellent method named Line3Dpp [36]. For datasets with depth images, we adopt a light-weight reconstruction method which maps 2D lines to 3D space directly. However, due to the depth discontinuities between foreground and background, wrong 3D lines are generated to affect the accuracy of lines. Thus, a PnP with RANSAC method is applied on database images to filter lines whose endpoints are outliers. In other words, if two endpoints of the line both are inliers, corresponding 2D-3D line matches of database images are reserved.

Finally, reprojection constraint is used to get high-quality 2D-3D line matches. Given coarse 2D-2D line matches between query and database images and accurate 2D-3D line correspondences of database image and 3D line map, the coarse line correspondence between 2D line in the query image and 3D line in the world coordinate system

is established. The reprojection error between the 3D line and corresponding 2D line on the query image with initial pose is computed which contains midpoint distance error and angle error that described in detail in Section III-C. The high-quality line matches with the lowest distance and angle error are selected as fine line matches. Fig.6 shows that our line matching method works well in some special scenes.

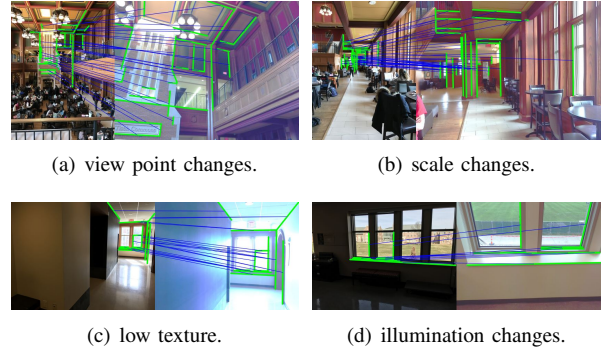


Fig. 6. **Result of line matching.** the evaluation of our line segments matching method works well in view point changes, scale changes, low texture and illumination changes.

C. POSE REFINEMENT WITH POINT-LINE

For each query image, the initial pose is achieved by our previous work, RLOCS [38], the pure point-based localization. The 2D-3D line correspondences of the query image and the 3D line Map are computed based on the initial pose, which is described in detail in Section III-B, denoted as $L_{corr} = \{(l_i, L_i)\}$. The query SE(3) pose is denoted as T , and the reprojection of the 3D line L_i on the query image plane is l'_i . The pose T is optimized by minimizing the midpoints distance error from l'_i to the corresponding 2D line l_i and the angle error between them. The linear equations of l_i and l'_i can be written as $Ax + By + C = 0$ and $A'x' + B'y' + C' = 0$. Then the cost function can be formulated as follows:

$$T^* = \arg \min_T \sum_{i=1}^N (\|d_i\| + \|\theta_i\|) \quad (5)$$

$$\|d_i\| = \|f(l_i) - f(h(K, T, L_i))\| \quad (6)$$

$$\|\theta_i\| = \frac{s|A_i B'_i - B_i A'_i|}{\sqrt{A_i^2 + B_i^2} \sqrt{A_i'^2 + B_i'^2}} \quad (7)$$

where N represents the number of 2D-3D line correspondences, the function $h(K, T, L_i)$ equals to l'_i , which represents the reprojection of 3D line L_i on the query image with pose T and intrinsic K . There are two endpoints on l'_i and the function $f(\cdot)$ represents the mean value of them, known as midpoint. The angle error $\|\theta_i\|$ is defined as the sine of the angle between l_i and l'_i . However, the metric of distance error $\|d_i\|$ is in pixel. In order to keep the metric of angle error consistent with distance error, we apply a scale factor s on the angle error. Different from the line prediction in Section III-A.1, here we use a scale factor to balance

the difference between the distance error and angle error by tuning the parameter, while during the model training this factor is hard to control and tuning. The distance error ensures that there is enough overlap between the line pair, meanwhile, the angle error ensures that their directions are closed to consistent. Our combined reprojection distance is better than the traditional distance which count the only distance from projected endpoints to the corresponding 2D line, by avoiding the singular condition where two lines are close to collinear but non-overlapping.

Due to the input coarse pose resulting in the different perspective between the query image and database images, the only line features are not stable enough in some certain scenes. Therefore, we propose a point-line joint optimization method that combining the traditional point reprojection constraints with the above line constraints to make the optimization more robust. While obtaining the initial pose, the 2D-3D inlier point correspondences involved in pose solver are also preserved, denoted as $P_{corr} = \{(p_j, P_j)\}$. Then the cost function evolves into the following form:

$$T^* = \arg \min_T (\alpha \sum_{i=1}^N (\|d_i\| + \|\theta_i\|) + \beta \sum_{j=1}^M \|e_j\|) \quad (8)$$

$$\|e_j\| = \|p_j - h(K, T, P_j)\| \quad (9)$$

where M represents the number of 2D-3D point correspondences. Similar to the formula 6, the function $h(K, T, P_j)$ represents the reprojection of 3D point P_j . In addition, two different weights α and β are applied to the lines and points reprojection error respectively to balance the weights of them. Usually, the ratio between α and β is fine-tuned based on the point and line correspondences numbers, and the sum of them equals 1 finally. The cost function is a nonlinear least squares problem and the Ceres-Solver [40] is employed to solve the optimized pose with the L-M algorithm and Huber loss function in our implementation.

IV. EXPERIMENTS

In this section, we evaluate the performance of line detection and point-line pose optimization respectively. All experiments are conducted on one NVIDIA Tesla V100 GPU with the CUDA 11.0 and Intel(R) Xeon(R) Glod 6142 CPU @ 2.60GHz.

A. Performance on Lines Detection

Wireframe [12] and YorkUrban [41] are typical line segment detection datasets. The following prevalent metrics are used in previous wireframe parser tasks [9], [12], [15]–[17], [20], and we evaluate our model with the structural Average Precision (sAP) [13], [42]. We conduct the experiments separately with the native Hourglass Network as the backbone and the one substituted with the Hybrid Block, which are abbreviated as VLSE_HG and VLSE_HG_HB respectively.

We compare our model with other line detection methods. Ours-HG denotes the model using Hourglass as the backbone to make a fair comparison to the one using the Hybrid Block, named as Ours-HG-HB. Table I summarizes the

results and comparisons based on sAP and AP^H . Ours-HG model achieves competitive performance with HAWP, and outperforms L-CNN in terms of sAP^{10} on Wireframe. Moreover, by changing the backbone from HG to HG-HB, we obtain the best results. For YorkUrban, Ours-HG-HB still reaches a comparable sAP result, which has only 0.1 decrease from the state-of-the-art result (LERT) in sAP^{10} .

TABLE I
QUANTITATIVE RESULTS AND COMPARISONS.

Method	Wireframe Dataset [12]			YorkUrban Dataset [41]		
	sAP^5	sAP^{10}	sAP^{15}	sAP^5	sAP^{10}	sAP^{15}
LSD [9]	6.7	8.8	/	7.5	9.2	/
DWP [12]	3.7	5.1	5.9	1.5	2.1	2.6
AFM [15]	18.5	24.4	27.5	7.3	9.4	11.1
L-CNN [13]	58.9	62.9	64.9	24.3	26.4	27.5
TP-LSD [17]	57.5	60.6	/	25.3	27.4	/
HAWP [16]	62.5	66.5	68.2	26.1	28.5	29.7
M-LSD [20]	56.4	62.1	/	24.6	27.3	/
LETR [42]	/	65.2	67.7	/	29.4	31.7
Ours-HG	61.1	66.1	68.4	25.1	27.5	29.1
Ours-HG-HB	62.1	67.3	69.6	26.6	29.3	30.9

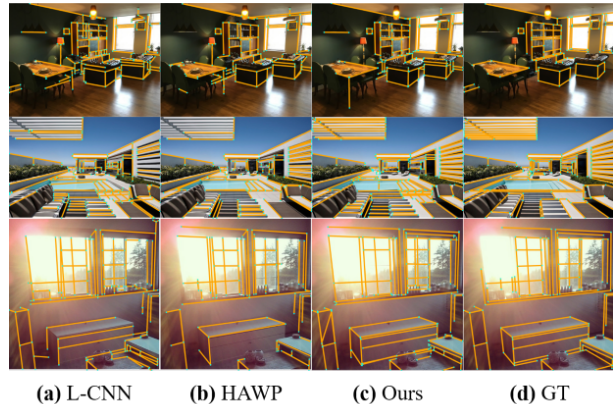


Fig. 7. **Qualitative evaluation of line segment detection methods on Wireframe dataset.** From left to right, the columns shows the results from (a) L-CNN [13], (b) HAWP [16], (c) Ours, and (d) the ground truth.

We also visualize the output of our VLSE and other methods L-CNN and HAWP in Fig.7. Junctions and line segments are colored with cyan blue and orange, respectively. L-CNN, which relies on the junctions detection and might be prone to the missed junctions and nearby texture variation, captures many messy lines. HAWP gives a relatively precise detection result but seems to miss some key line segments.

B. Performance on Localization

We validate our pose optimization method on the public Long-Term Visual Localization benchmark. Two typical datasets, Aachen Day-Night v1.1 and InLoc are selected for experiments. Aachen Day-Night v1.1 dataset is an outdoor scene with a SFM model and InLoc dataset is an indoor scene with depth images. For different characteristics of the two

datasets, the 3D line map of Aachen is built by COLMAP [7] and Line3Dpp [36] with LSD line extraction method, because the line extracted by VLSE is complete and non-repetitive so that it is not friendly enough to the line tracking. The InLoc 3D line map is reconstructed by projecting the VLSE extracted 2D lines into depth images. The both 3D line maps are visualized respectively in Fig.8.

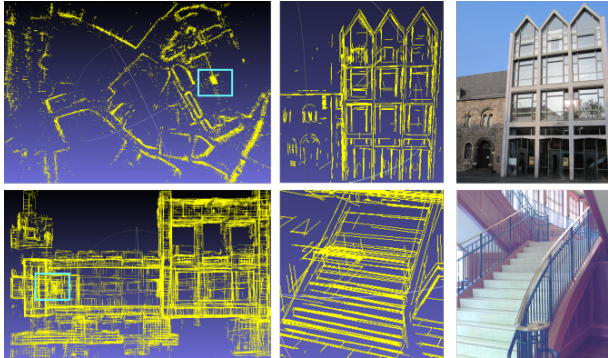


Fig. 8. **Results of line mapping.** The first and second row represent the result of line map of Aachen Day-Night v1.1 and InLoc respectively. The first column represents a bird’s-eye view, the second and the third column show the zoomed view of details and the actual scene.

Our previous work, RLOCS [38], provides the latest localization results as the initial poses of our optimization and the inliers involved in pose solver are also saved to join to point-line joint optimization. The localization performance is shown in the score on the online list. In order to verify the improvement of localization accuracy caused by line optimization and point-line joint optimization, which corresponds to Eq.5 and Eq.8, we conduct the experiments on above two datasets under the different cost functions with the same initial poses. The results are shown in Table II.

TABLE II

POINT-LINE POSE OPTIMIZATION ON *Aachen Day-Night v1.1* AND *InLoc*

<i>Aachen Day-Night v1.1</i>	<i>day</i>		<i>night</i>	
	(0.25m, 2°) / (0.5m, 5°) / (5m, 10°)			
Baseline	89.8 / 96.7 / 99.5	74.9 / 90.6 / 100.0		
Line Optimization	89.7 / 96.7 / 99.5	75.4 / 90.6 / 100.0		
Point-Line Joint Optimization	90.0 / 96.7 / 99.5	80.6 / 92.1 / 100.0		
<i>InLoc</i>	<i>duc1</i>		<i>duc2</i>	
	(0.25m, 10°) / (0.5m, 10°) / (1m, 10°)			
BaseLine	47.0 / 71.2 / 84.8	61.1 / 77.9 / 80.2		
Line Optimization	51.5 / 71.7 / 84.3	61.8 / 78.6 / 80.9		
Point-Line Joint Optimization	50.5 / 72.7 / 86.9	61.8 / 79.4 / 84.0		

For Aachen Day-Night v1.1, the improvement of localization performance is not obvious by line optimization, except in the first column on *night* dataset. Some cases are closed to the ground truth while some get far away from it after optimization due to the individual line constraints are not comprehensive enough. However the results of point-line joint optimization are generally improved, especially on *night* dataset. For InLoc, the localization performance by line

optimization is better than baseline and there is a significant improvement at accuracy (0.25m, 2°) on *duc1*. In addition, the result is further improved in different accuracy ranges after point-line joint optimization.

Moreover, we compare our point-line joint pose optimization method with various typical approaches on the Long-Term Visual Localization benchmark. The latest results of some outstanding approaches with publication are captured from visuallocalization.net/benchmark/ and shown in the Table III. We found that our point-line joint optimization result named PtLine in benchmark list can not only improve the performance based on the baseline, but also can perform well in various excellent methods.

TABLE III

EVALUATION OF STATE-OF-THE-ART APPROACHES ON *Aachen Day-Night v1.1* AND *InLoc*

<i>Aachen Day-Night v1.1</i>	<i>day</i>		<i>night</i>	
	(0.25m, 2°) / (0.5m, 5°) / (5m, 10°)			
KAPTURE-R2D2-APGeM [34]	90.0 / 96.2 / 99.5	72.3 / 86.4 / 97.9		
LoFTR [6]	88.7 / 95.6 / 99.0	78.5 / 90.6 / 99.0		
SuperGlue+Patch2Pix [5] [43]	89.3 / 95.8 / 99.2	78.0 / 90.6 / 99.0		
HLoc-SuperPoint+SuperGlue [5]	89.8 / 96.1 / 99.4	77.0 / 90.6 / 100.0		
KAPTURE-R2D2-FUSION [34]	90.9 / 96.7 / 99.5	78.5 / 91.1 / 98.4		
RLOCS-v3.0 [38]	89.8 / 96.7 / 99.5	74.9 / 90.6 / 100.0		
Ours (PtLine)	90.0 / 96.7 / 99.5	80.6 / 92.1 / 100.0		
<i>InLoc</i>	<i>duc1</i>		<i>duc2</i>	
	(0.25m, 10°) / (0.5m, 10°) / (1m, 10°)			
KAPTURE-R2D2-FUSION [34]	41.4 / 60.1 / 73.7	47.3 / 67.2 / 73.3		
DensePE+SNCNet+DensePV [44]	47.0 / 67.2 / 79.8	43.5 / 64.9 / 80.2		
HLoc-SuperPoint+SuperGlue [5]	49.0 / 68.7 / 80.8	53.4 / 77.1 / 82.4		
SuperGlue+Patch2Pix [5] [43]	50.0 / 68.2 / 81.8	57.3 / 77.9 / 80.2		
LoFTR [6]	47.5 / 72.2 / 84.8	54.2 / 74.8 / 85.5		
RLOCS-v3.0 [38]	47.0 / 71.2 / 84.8	61.1 / 77.9 / 80.2		
Ours (PtLine)	50.5 / 72.7 / 86.9	61.8 / 79.4 / 84.0		

V. CONCLUSIONS

In conclusion, we propose a novel point-line optimization method for pose refinement in this work. We design a more accurate and stable line extractor CNN for the following line matching and mapping process. We adopt a coarse-to-fine line matching method based on epipolar constraint with large line reprojection error filtering to get high-quality line matches. In addition, we establish a point-line joint cost function to optimize the query pose with an initial value obtained from the only-point localization. Sufficient experiments are conducted on Aachen Day-Night v1.1 and InLoc to confirm the effectiveness and superiority of our proposed method. The pipeline is highly modular and extensible. In future, we look forward to further improvement of line extraction CNN by extending the training datasets into outdoor scenes, and escalating line matching and optimization strategy to reach the better localization precision.

REFERENCES

- [1] H. Lim, S. N. Sinha, M. F. Cohen, and M. Uyttendaele, "Real-time image-based 6-dof localization in large-scale environments," in *2012 IEEE conference on computer vision and pattern recognition*, pp. 1043–1050, IEEE, 2012.
- [2] R. Castle, G. Klein, and D. W. Murray, "Video-rate localization in multiple maps for wearable augmented reality," in *2008 12th IEEE International Symposium on Wearable Computers*, pp. 15–22, IEEE, 2008.
- [3] D. DeTone, T. Malisiewicz, and A. Rabinovich, "Superpoint: Self-supervised interest point detection and description," in *Proceedings of the IEEE conference on computer vision and pattern recognition workshops*, pp. 224–236, 2018.
- [4] J. Revaud, P. Weinzaepfel, C. De Souza, N. Pion, G. Csurka, Y. Cabon, and M. Humenberger, "R2d2: repeatable and reliable detector and descriptor," *arXiv preprint arXiv:1906.06195*, 2019.
- [5] P.-E. Sarlin, D. DeTone, T. Malisiewicz, and A. Rabinovich, "Superglue: Learning feature matching with graph neural networks," in *Proceedings of the IEEE/CVF conference on computer vision and pattern recognition*, pp. 4938–4947, 2020.
- [6] J. Sun, Z. Shen, Y. Wang, H. Bao, and X. Zhou, "Loftr: Detector-free local feature matching with transformers," *CoRR*, vol. abs/2104.00680, 2021.
- [7] J. L. Schonberger and J.-M. Frahm, "Structure-from-motion revisited," in *Proceedings of the IEEE conference on computer vision and pattern recognition*, pp. 4104–4113, 2016.
- [8] P. Moulon, P. Monasse, R. Perrot, and R. Marlet, "Openmvg: Open multiple view geometry," in *International Workshop on Reproducible Research in Pattern Recognition*, pp. 60–74, Springer, 2016.
- [9] R. G. Von Gioi, J. Jakubowicz, J.-M. Morel, and G. Randall, "Lsd: A fast line segment detector with a false detection control," *IEEE transactions on pattern analysis and machine intelligence*, vol. 32, no. 4, pp. 722–732, 2008.
- [10] J. H. Lee, S. Lee, G. Zhang, J. Lim, W. K. Chung, and I. H. Suh, "Outdoor place recognition in urban environments using straight lines," in *2014 IEEE International Conference on Robotics and Automation (ICRA)*, pp. 5550–5557, IEEE, 2014.
- [11] C. Akinlar and C. Topal, "Edlines: A real-time line segment detector with a false detection control," *Pattern Recognition Letters*, vol. 32, no. 13, pp. 1633–1642, 2011.
- [12] K. Huang, Y. Wang, Z. Zhou, T. Ding, S. Gao, and Y. Ma, "Learning to parse wireframes in images of man-made environments," in *Proceedings of the IEEE Conference on Computer Vision and Pattern Recognition*, pp. 626–635, 2018.
- [13] Y. Zhou, H. Qi, and Y. Ma, "End-to-end wireframe parsing," in *Proceedings of the IEEE/CVF International Conference on Computer Vision*, pp. 962–971, 2019.
- [14] Z. Zhang, Z. Li, N. Bi, J. Zheng, J. Wang, K. Huang, W. Luo, Y. Xu, and S. Gao, "Ppgnet: Learning point-pair graph for line segment detection," in *Proceedings of the IEEE/CVF Conference on Computer Vision and Pattern Recognition*, pp. 7105–7114, 2019.
- [15] N. Xue, S. Bai, F. Wang, G.-S. Xia, T. Wu, and L. Zhang, "Learning attraction field representation for robust line segment detection," in *Proceedings of the IEEE/CVF Conference on Computer Vision and Pattern Recognition*, pp. 1595–1603, 2019.
- [16] N. Xue, T. Wu, S. Bai, F. Wang, G.-S. Xia, L. Zhang, and P. H. Torr, "Holistically-attracted wireframe parsing," in *Proceedings of the IEEE/CVF Conference on Computer Vision and Pattern Recognition*, pp. 2788–2797, 2020.
- [17] S. Huang, F. Qin, P. Xiong, N. Ding, Y. He, and X. Liu, "Tp-lsd: Tri-points based line segment detector," in *Computer Vision—ECCV 2020: 16th European Conference, Glasgow, UK, August 23–28, 2020, Proceedings, Part XXVII 16*, pp. 770–785, Springer, 2020.
- [18] X. Dai, X. Yuan, H. Gong, and Y. Ma, "Fully convolutional line parsing," *arXiv preprint arXiv:2104.11207*, 2021.
- [19] H. Zhang, Y. Luo, F. Qin, Y. He, and X. Liu, "Elsd: Efficient line segment detector and descriptor," *arXiv preprint arXiv:2104.14205*, 2021.
- [20] G. Gu, B. Ko, S. Go, S.-H. Lee, J. Lee, and M. Shin, "Towards real-time and light-weight line segment detection," *arXiv preprint arXiv:2106.00186*, 2021.
- [21] X.-S. Gao, X.-R. Hou, J. Tang, and H.-F. Cheng, "Complete solution classification for the perspective-three-point problem," *IEEE transactions on pattern analysis and machine intelligence*, vol. 25, no. 8, pp. 930–943, 2003.
- [22] M. A. Fischler and R. C. Bolles, "Random sample consensus: a paradigm for model fitting with applications to image analysis and automated cartography," *Communications of the ACM*, vol. 24, no. 6, pp. 381–395, 1981.
- [23] A. Newell, K. Yang, and J. Deng, "Stacked hourglass networks for human pose estimation," in *European conference on computer vision*, pp. 483–499, Springer, 2016.
- [24] C. Schmid and A. Zisserman, "The geometry and matching of lines and curves over multiple views," *International Journal of Computer Vision*, vol. 40, no. 3, pp. 199–233, 2000.
- [25] R. I. Hartley, "A linear method for reconstruction from lines and points," in *Proceedings of IEEE International Conference on Computer Vision*, pp. 882–887, IEEE, 1995.
- [26] L. Zhang and R. Koch, "An efficient and robust line segment matching approach based on lbd descriptor and pairwise geometric consistency," *Journal of Visual Communication and Image Representation*, vol. 24, no. 7, pp. 794–805, 2013.
- [27] Q. Ma, G. Jiang, and D. Lai, "Robust line segments matching via graph convolution networks," *arXiv preprint arXiv:2004.04993*, 2020.
- [28] R. Pautrat, J.-T. Lin, V. Larsson, M. R. Oswald, and M. Pollefeys, "Sold2: Self-supervised occlusion-aware line description and detection," in *Proceedings of the IEEE/CVF Conference on Computer Vision and Pattern Recognition*, pp. 11368–11378, 2021.
- [29] P. Smith, I. D. Reid, and A. J. Davison, "Real-time monocular slam with straight lines," 2006.
- [30] R. Gomez-Ojeda, F.-A. Moreno, D. Zuniga-Noël, D. Scaramuzza, and J. Gonzalez-Jimenez, "PI-slam: A stereo slam system through the combination of points and line segments," *IEEE Transactions on Robotics*, vol. 35, no. 3, pp. 734–746, 2019.
- [31] A. Pumarola, A. Vakhitov, A. Agudo, A. Sanfeliu, and F. Moreno-Noguer, "PI-slam: Real-time monocular visual slam with points and lines," in *2017 IEEE international conference on robotics and automation (ICRA)*, pp. 4503–4508, IEEE, 2017.
- [32] X. Wei, J. Huang, and X. Ma, "Real-time monocular visual slam by combining points and lines," in *2019 IEEE International Conference on Multimedia and Expo (ICME)*, pp. 103–108, IEEE, 2019.
- [33] Y. He, J. Zhao, Y. Guo, W. He, and K. Yuan, "PI-vio: Tightly-coupled monocular visual-inertial odometry using point and line features," *Sensors*, vol. 18, no. 4, p. 1159, 2018.
- [34] M. Humenberger, Y. Cabon, N. Guerin, J. Morat, J. Revaud, P. Re-role, N. Pion, C. de Souza, V. Leroy, and G. Csurka, "Robust image retrieval-based visual localization using kapture," *arXiv preprint arXiv:2007.13867*, 2020.
- [35] L. Zhou, S. Wang, and M. Kaess, "A fast and accurate solution for pose estimation from 3d correspondences," in *2020 IEEE International Conference on Robotics and Automation (ICRA)*, pp. 1308–1314, IEEE, 2020.
- [36] M. Hofer, M. Maurer, and H. Bischof, "Efficient 3d scene abstraction using line segments," *Computer Vision and Image Understanding*, vol. 157, pp. 167–178, 2017.
- [37] C. Szegedy, W. Liu, Y. Jia, P. Sermanet, S. Reed, D. Anguelov, D. Erhan, V. Vanhoucke, and A. Rabinovich, "Going deeper with convolutions," in *Proceedings of the IEEE conference on computer vision and pattern recognition*, pp. 1–9, 2015.
- [38] Y. Zhou, H. Fan, S. Gao, Y. Yang, X. Zhang, J. Li, and Y. Guo, "Retrieval and localization with observation constraints," *arXiv preprint arXiv:2108.08516*, 2021.
- [39] A. M. Andrew, "Multiple view geometry in computer vision," *Kybernetes*, 2001.
- [40] S. Agarwal, K. Mierle, and Others, "Ceres solver." <http://ceres-solver.org>.
- [41] P. Denis, J. H. Elder, and F. J. Estrada, "Efficient edge-based methods for estimating manhattan frames in urban imagery," in *European conference on computer vision*, pp. 197–210, Springer, 2008.
- [42] Y. Xu, W. Xu, D. Cheung, and Z. Tu, "Line segment detection using transformers without edges," in *Proceedings of the IEEE/CVF Conference on Computer Vision and Pattern Recognition*, pp. 4257–4266, 2021.
- [43] Q. Zhou, T. Sattler, and L. Leal-Taixe, "Patch2pix: Epipolar-guided pixel-level correspondences," 2021.
- [44] I. Rocco, R. Arandjelović, and J. Sivic, "Efficient neighbourhood consensus networks via submanifold sparse convolutions," in *European Conference on Computer Vision*, 2020.